Journal of Magnetic Resonance **146,** 260–276 (2000)
doi:10.1006/jmre.2000.2154, available online at http://www.idealibrary.com on IDEAL®

# A Comprehensive Approach for Accurate Measurement of Proton–Proton Coupling Constants in the Sugar Ring of DNA

Jiping Yang,*[,1] Kathleen McAteer,* Louis A. "Pete" Silks,† Ruilian Wu,† Nancy G. Isern,* Clifford J. Unkefer,† and Michael A. Kennedy*[,2]

*Environmental Molecular Sciences Laboratory, Pacific Northwest National Laboratory, Richland, Washington 99352; and †National Stable Isotopes Laboratory, Los Alamos National Laboratory, Los Alamos, New Mexico 87545

Received March 4, 2000; revised June 27, 2000

**Stereo-selective deuteration has been explored as an approach for improving the accuracy of NMR-derived, three-bond vicinal proton–proton coupling constants in the 12-base-pair DNA Dickerson sequence [*d*(CGCGAATTCGCG)$_2$]. The coupling constants are useful for DNA structure determination in restrained molecular dynamics calculations. Specifically, the A5 and A6 residues were prepared with the H2″ proton stereo-selectively replaced with a deuteron. Deuteration of the H2″ leads to a 42-fold reduction in the transverse cross-relaxation rate of the H2′ spin, effectively negating the contribution of transverse cross relaxation to the cross peak frequencies and phases. Calculated linewidth and polarization transfer functions indicated that the reduced dipolar interaction is also expected to result in a significant increase in intensity for all cross peaks involving the H1′, H2′, or H3′ spin. The spectral complexity is also reduced by selective deuteration. Time-shared homonuclear decoupling of passive spins during acquisition was implemented, reducing the spin system, in some cases, to an effectively isolated two-spin system. This enables the use of a 90° mixing pulse instead of the 35° pulse commonly used in standard P.E.COSY experiments, leading to an additional 75% increase in signal intensity. Selective excitation pulses were used to reduce the number of increments required in the indirect dimension by as much as a factor of 4. The cumulative improvement in sensitivity is striking, approaching three orders of magnitude per unit time. Separate experiments, referred to as Stripe-COSY and Superstripe-COSY, were optimized for each coupling constant measured. Finally, *J*-doubling was used to obtain the most accurate peak separations. This comprehensive approach shows promise as an effective method for extracting highly accurate homonuclear vicinal coupling constants in DNA.** 

*Key Words:* **coupling constants; DNA; *J* doubling; selective deuteration; Stripe-COSY.**

## INTRODUCTION

Three-bond homonuclear and heteronuclear vicinal coupling constants have been widely used for the conformational analysis of biomacromolecules since their values can be related to three-bond torsion angles via Karplus relationships (*1*). The application of such relationships to biomacromolecules is complicated because these molecules typically tumble in solution with autocorrelation times in the spin-diffusion limit ($\omega\tau_c \gg 1$). The correspondingly short transverse relaxation times produce resonance linewidths that frequently approach or exceed the size of the coupling constant of interest. Furthermore, biomacromolecules typically have high local proton densities so that $^1$H relaxation is dominated by dipolar interactions with other protons (within approximately 5 Å), which leads to efficient dipolar relaxation and corresponding broad resonance lines (*2*). Consequently, broad lines, spectral overlap, weak signals, and transverse cross-relaxation effects complicate the process of extracting meaningful values for coupling constants derived from NMR spectra. Drobny and co-workers have highlighted the conditions for extracting accurate coupling constants from DNA duplexes with longer correlation times from P.E.COSY type data (*3*). It has also been demonstrated theoretically that relaxation effects can preclude the accurate measurement of coupling constants from E.COSY spectra due to differential relaxation of double- and triple-quantum coherences (*4, 5*).

The problem associated with overlapped cross peaks can be overcome to a certain extent by E.COSY (*6*) or P.E.COSY (*7*)-type experiments in which the number of multiplet components in each cross peak is reduced to the number of connected transitions. For a three-spin system, the number of cross-peak multiplets is reduced from 16 to 8 in the form of two quartets displaced by the passive coupling constants. Both active and passive coupling constants can be measured directly from the E.COSY or the P.E.COSY spectrum. The disadvantage of E.COSY lies in its complicated data acquisition process, which requires the linear combination of multiple phase-shifted data sets. This increases both the minimum acquisition time and susceptibility to spectrometer instabilities. The P.E.COSY is much easier to run experimentally since it requires only two pulses. However, the 35° mixing pulse (which intrinsically produces less signal than a 90° pulse) and the use of two alternating phase cycling schemes to remove the dis-

[1] Current address: Hoechst Marrion Roussel Inc., 1041 Route 202-206, P.O. Box 6800, Bridgewater, New Jersey 08807.

[2] To whom correspondence should be addressed. Fax: (509) 376-2303. E-mail: ma_kennedy@pnl.gov.



1090-7807/00 $35.00

persive character of the diagonal autopeaks make the P.E.COSY experiment lengthy, especially when significant signal averaging is required to produce a spectrum with a good signal-to-noise ratio. In order to reduce the total acquisition time, we have recently reported the use of the Stripe-COSY experiment (*8*), which is a P.E.COSY experiment utilizing selective excitation to the particular region of the spectrum of interest. Up to a fourfold savings in time has been demonstrated for measurement of the H1′–H2′ three-bond coupling constants for the 12-base-pair [*d*(CGCGAATTCGCG)$_2$] Dickerson DNA sequence. We have also introduced the Superstripe-COSY experiment (*8*), which is a general name for a P.E.COSY experiment employing both selective excitation of active spins and selective decoupling to collapse key passive couplings. The result leads to enhanced signal-to-noise and decreased overlap of intracross-peak multiplet components.

Transverse cross relaxation has been shown to modulate both the frequency and phase of cross peak components (*9*) and can be significant when one of the active spins is one of a pair of geminal protons on a methylene carbon, such as the geminal H2′–H2″ pair at the C2′ carbon in the deoxyribose sugar of DNA, or at a methylene carbon in a protein side chain. In DNA, three out of the four three-bond coupling constants related to the sugar conformation involve either the geminal H2′ or H2″ proton. Therefore, neglect of transverse cross-relaxation effects, either in spectral simulations or when interpreting peak separations, can potentially lead to misinterpretation of DNA sugar conformation analyses. We have recently proposed an approach for directly probing the effect of transverse cross relaxation on coupling constants involving either the H2′ or H2″ proton in DNA and for eliminating the effects of transverse cross relaxation. The approach involves stereospecific deuteration of one of the geminal protons, thereby reducing the cross-relaxation rate by the square of the ratio of the gyromagnetic ratios, i.e., $(\gamma D/\gamma H)^2$ or about 42-fold. The effect of deuteration on the resonance linewidths was dramatic, producing an 8–9-fold increase in signal-to-noise for the H1′–H2′ cross peak. In fact, the resonance lines sharpened sufficiently so that a discontinuity between antiphase components was observed, indicating that frequency shifts of component minima and maxima due to the effects of self-cancelation could be ignored and the value of the coupling constant measured directly from the splitting of the antiphase components. The use of nonstereospecific, partially deuterated nucleotide residues in DNA to obtain accurate and unambiguous $^3J_{H1'-H2'}$ and $^3J_{H1'-H2''}$ coupling constant information for DNA as large as 20 base pairs has been demonstrated elsewhere (*10*).

There are several post-acquisition processing methods available for separation of unresolved splitting, including maximum entropy reconstruction (*11*, *12*), *J* deconvolution (*13*, *14*), and *J* doubling (*15*, *16*). Among them, the *J* doubling is a relatively straightforward and reliable method. However, since each stage of the *J* doubling reduces the signal-to-noise ratio by a factor of 2, a favorable starting signal-to-noise ratio is required. Fortunately, the improvements in signal to noise ratio realized when Superstripe-COSY is used together with selective deuteration can lead to 2–3 orders of magnitude increase in signal-to-noise per unit time. Therefore, *J* doubling may be quite useful in these circumstances.

In our previous Communication (*8*), we demonstrated the improvement in sensitivity for measuring three-bond proton–proton coupling constants due to the combined use of stereoselective deuterium labeling, time-shared homonuclear decoupling, and selective excitation schemes. In this paper, a comprehensive approach for measuring $^3J_{HH}$ extracted from NMR data with the highest possible accuracy and sensitivity is outlined. Various stereo-selective deuterium-labeling schemes are considered, and spin–spin relaxation times and polarization transfer functions are calculated for each labeling pattern. Implementation of *J* doubling in crowded regions is illustrated using trapezoid apodization to simplify and improve the *J*-doubling analysis. Finally, $^3J_{H1'-H2'}$, $^3J_{H2'-H3'}$, and $^3J_{H3'-H4'}$ coupling constants were measured employing selective deuteration, Superstripe-COSY, and *J* doubling and the results compared with the coupling constant measurements and analyses of the sugar conformations reported elsewhere.

## RESULTS

### *Selection of Coupling Constants for Measurement*

There are five protons on the furanose sugar ring of DNA (Fig. 1). Two protons occur as a geminal pair at the C2′ carbon. Stereo-selective replacement of one geminal proton by deuterium at the C2′ carbon eliminates the strong geminal proton coupling, leaving three vicinal couplings to determine the sugar conformation. At the C2′ carbon, either the H2′ or the H2″ proton is a candidate for replacement by deuterium. Therefore it is worthwhile to consider which combinations of coupling constants are most sensitive to the sugar conformation. Figure 2 shows how the three-bond coupling constants depend on the pseudorotation phase angle (*P*). The curves were calculated using the most recently optimized Karplus coefficients taken from PSEUROT v6.2 (J. Van Wijk and C. Altona, Leiden Institute of Chemistry, Leiden University). If the H2″ proton is replaced by a deuteron, three measurable proton–proton vicinal couplings remain: $^3J_{H1'-H2'}$, $^3J_{H2'-H3'}$, and $^3J_{H3'-H4'}$. Inspection of the Karplus curves shows that the $^3J_{H1'-H2'}$ constant is only weakly dependent on *P* in the range of pseudorotation phase angles normally found in the south conformation from $P = 130°$ to 180°. However, since $^3J_{H1'-H2'}$ differs by nearly 10 Hz between north ($P \sim 0°$) and south ($P \sim 162°$) sugar conformations, it should be sensitive to relative populations of north and south conformers. In contrast, if the H2′ proton is replaced by a deuteron, only the vicinal coupling involving the H1′ proton corresponding to the $^3J_{H1'-H2''}$ coupling constant (correlated with the $\nu_1$ torsion angle) would remain, which gives little difference (1–2 Hz) between north and south

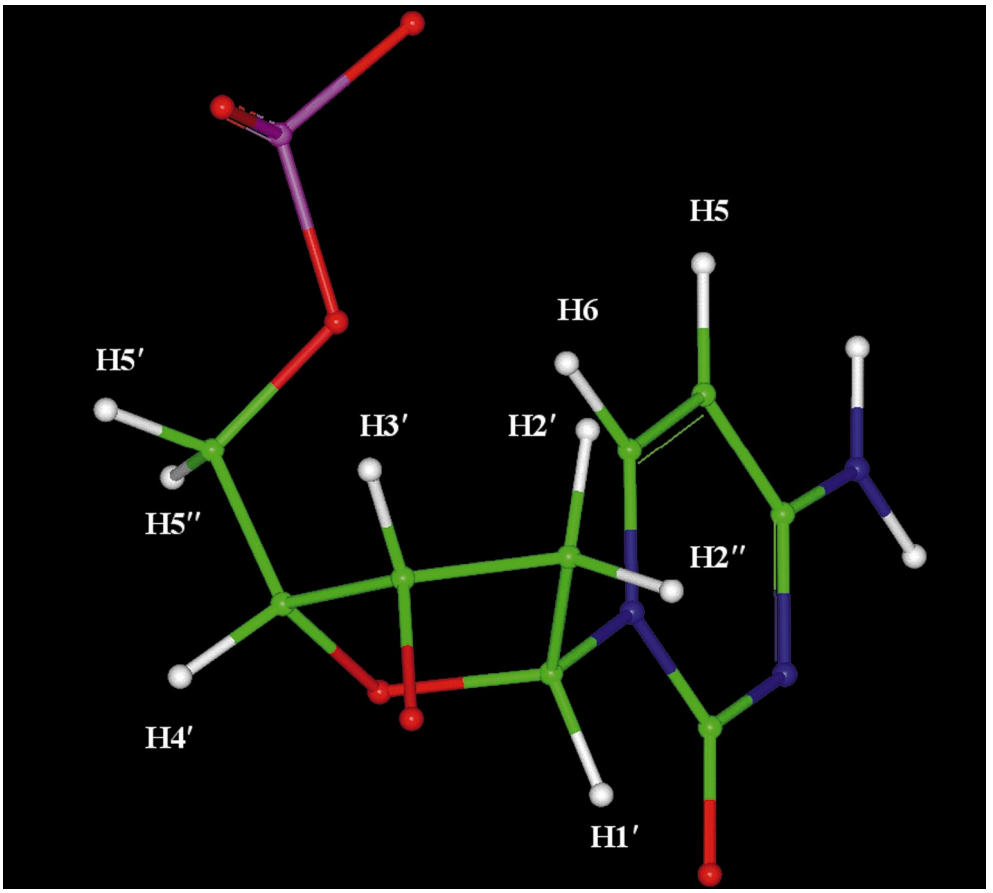


**FIG. 1.** Schematic representation of the topology of protons in a deoxyribose sugar fragment in DNA.

conformers with values of ~7 Hz (north) and 5–6 Hz (south), respectively, and is therefore less sensitive. The $^3J_{H2'-H3'}$ coupling varies from ~5.5 to 7.5 Hz over $P = 130°$ to 180°. However, the magnitude of $^3J_{H2''-H3'}$ (the remaining vicinal coupling if the H2′ proton were replaced by a deuteron) differs by nearly 10 Hz between north (~10 Hz) and south (~1 Hz) conformers. Finally, the $^3J_{H3'-H4'}$ coupling constant, like the $^3J_{H1'-H2'}$ coupling constant, is very sensitive to $P$ with values of ~9 Hz for north and 1–3.5 Hz (south).

Replacing the H2″ with a deuteron is therefore the most effective choice to derive structural information on the sugar conformation in DNA since: (1) the sugar conformations are predominantly south in DNA; (2) the $^3J_{H1'-H2'}$ is more sensitive to differences between north and south conformers; and (3) the magnitude of the $^3J_{H2'-H3'}$ is measurable in the south range, whereas the $^3J_{H2''-H3'}$ would not be of sufficient magnitude to measure.

### *Experimental Strategy for Measuring Three-Bond Proton–Proton Coupling Constants in DNA*

As mentioned above, cross-peak overlap, broad lines, and transverse cross relaxation between geminal protons pose the most serious problems for accurate determination of $^3J_{HH}$ in DNA. We outline a strategy that combines three different approaches for minimizing the impact of these factors: (1) selective deuteration/exchange, (2) selective excitation/decoupling, and (3) deconvolution via $J$ doubling.

*(1) Selective deuteration/exchange.* The first approach is aimed at minimizing dipolar interactions that cause significant line broadening by stereo-selective deuteration and selective deuterium exchange. Table 1 summarizes all interproton distances less than 5 Å in canonical B-DNA. Figure 3 shows how the linewidth for the H1′ (Fig. 3A), H2′ (Fig. 3C), H3′ (Fig. 3E), and H4′ (Fig. 3G) protons depends on the correlation time, taking into account all spins closer than 2, 3, <4, and <5 Å, respectively. From Fig. 3, it is apparent that the proton linewidths are dominated by dipolar interactions with other protons that are closer than 2 Å. For the most part, these interactions are limited to geminal pairs of protons and some H8/H6 to H2′ distances (See Table 1). Therefore, selective deuteration at geminal proton pairs occurring at the C2′ and C5′ carbons can be very effective in reducing proton–proton linewidths in DNA (*8*). Replacing the adenine H8 with a deuteron also has potential beneficial applications and can be

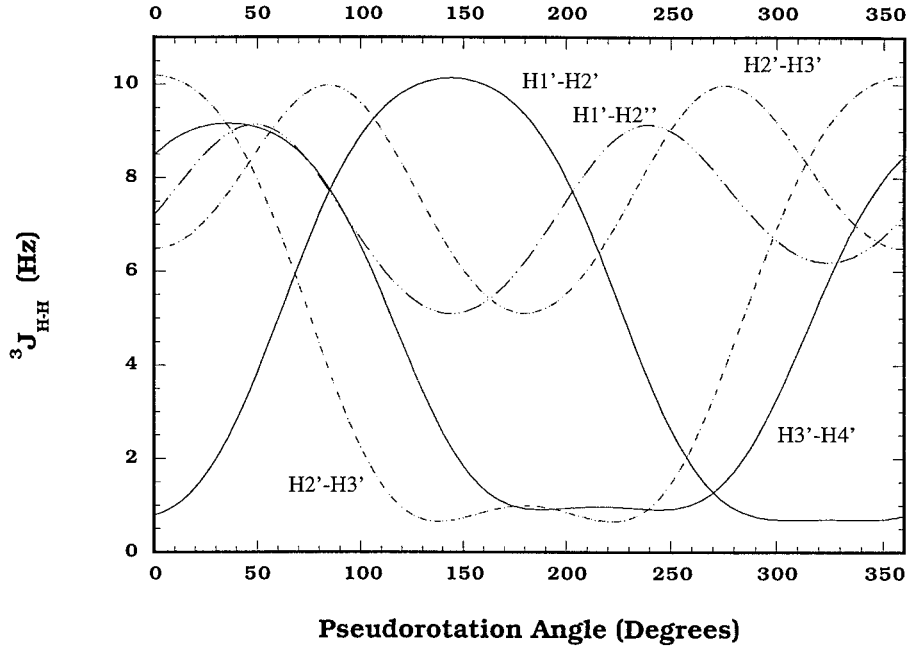


**FIG. 2.** Calculated vicinal three-bond proton–proton coupling constants as a function of pseudorotation angle (*P*).

easily accomplished since the H8 proton of purines is readily exchangeable at raised temperatures. Proton linewidths (Fig. 3) were calculated assuming either selective deuteration of the H2″ proton or deuteration at the H8 position. The magnitude of the linewidth reduction depends on the proximity of other protons for each proton type considered. For example, the H2′ proton, with its nearest neighbor proton H2″ only 1.76 Å away, benefits the most by replacement of the H2″ proton by a deuteron, which results in a linewidth reduction of nearly 75% (from ~45 to ~10 Hz at $\tau_c$ = 10 ns). In contrast, the H3′ proton experiences only a relatively modest (~33%) reduction in linewidth from ~12 to ~8 Hz for an H2″ to D″ replacement. The reduction of the H1′ and H4′ linewidths falls in between the predicted values for the H2′ and H3′ protons.

The impact of the effective spin–spin relaxation of the polarization transfer efficiencies is illustrated in Fig. 4. Stripe-COSY cross peaks, such as the H1′–H2′ cross-peak, originate from the evolution of antiphase magnetization, which contains a transverse component of magnetization for the selectively excited region, e.g., $^{H1'}I_{x,y}$, before the mixing pulse. The relevant coherence transfer function is an exponentially decaying function of the $T_2$ of the transverse component of the magnetization before the mixing pulse. Therefore, using the proton linewidths calculated above, it is possible to calculate the coherence transfer functions under a variety of theoretical labeling patterns, as summarized in Fig. 4. For example, based on the relative intensity of the transfer functions (see Figs. 4A and 4B) a signal enhancement of ~50% is predicted for the H1′–H2′ cross peak in a sample where the H2″ and H8 protons are replaced with deuterons in comparison to a sample in which all protons within 5 Å are considered. An even greater effect is predicted for cross peaks involving transverse magnetization of the H2′ spin, where the intensity of the transfer function is enhanced by >100% (see Figs. 4C and 4D) from a maximum value of 0.4 to 1.4 with stereo-selective deuteration at the H2″ site. A further 57% increase is obtained if the H8 proton is exchanged with a deuteron. A cumulative enhancement of ~62% is predicted for cross peaks involving transverse H3′ proton magnetization.

Therefore, the most general strategy for minimizing dipolar interactions in DNA, while leaving key protons required for analysis of sugar conformations, is to prepare oligonucleotides in which all base protons are replaced by deuterons, and where the C2′ and C5′ carbons are prepared stereo-selectively with deuterium, eliminating strongly coupled geminal pairs of protons. Using this strategy, two samples would be required for complete structure analysis: one sample with stereo-selective deuteration limited to the sugar ring for NOESY data sets, and a second sample deuterated both in the sugar and bases for optimal measurement of sugar conformations.

*(2) Selective excitiation/decoupling.* The second approach employs band-selective excitation and band-selective homonuclear and/or heteronuclear decoupling during the acquisition. Since the direct detection dimension, F2, has higher intrinsic digital resolution than the indirect F1 dimension, it is preferable to measure coupling constants in F2. This is an important consideration when designing a Stripe-COSY- or Superstripe-COSY-type experiment, since it is desirable to measure the relevant splitting in the highest resolution dimension. Table 2 summarizes this approach for measurement of the $^3J_{H1'-H2'}$, $^3J_{H2'-H3'}$, and $^3J_{H3'-H4'}$ coupling constants. Figure 5 illustrates the

**TABLE 1**
**Proton–Proton Distances Taken from a Canonical Model of a *d*(GAA) Segment**

| | H1′ | H2′ | H2″ | H3′ | H4′ | H5′ | H5″ |
|---|---|---|---|---|---|---|---|
| H1′($i$ − 1) | 4.92 | 4.14 | > | 4.96 | 4.24 | 1.81[a] | 3.36 |
| H2′($i$ − 1) | > | > | > | > | > | 4.49 | > |
| H2″($i$ − 1) | > | 3.84 | > | > | > | 3.41 | 4.09 |
| H3′($i$ − 1) | > | > | > | > | > | 4.59 | 4.77 |
| H4′($i$ − 1) | > | > | > | > | > | 3.84 | 4.19 |
| H1′ | X | 3.03 | 2.37 | 3.93 | 3.65 | 4.46 | > |
| H2′ | 3.03 | X | 1.76 | 2.40 | 3.86 | 3.82 | 3.90 |
| H2″ | 2.37 | 1.76 | X | 2.70 | 4.09 | 4.96 | 4.94 |
| H3′ | 3.93 | 2.40 | 2.70 | X | 2.65 | 3.75 | 2.83 |
| H4′ | 3.65 | 3.86 | 4.09 | 2.65 | X | 2.60 | 2.29 |
| H5′ | 4.46 | 3.82 | 4.96 | 3.75 | 2.60 | X | 1.78 |
| H5″ | > | 3.90 | 4.94 | 2.83 | 2.29 | 1.78 | X |
| H8 | 3.88 | 2.16 | 3.67 | 4.18 | 4.82 | 3.52 | 4.34 |
| H8($i$ + 1) | 2.83 | 3.70 | 2.29 | 4.95 | > | > | > |
| H5′($i$ + 1) | 1.81[a] | 4.49 | 3.41 | 4.59 | 3.84 | > | > |
| H5″($i$ + 1) | 3.36 | > | 4.09 | 4.77 | 4.19 | > | > |
| H4′($i$ + 1) | 4.24 | | | | | | |
| H3′($i$ + 1) | 4.96 | | | | | | |
| H2′($i$ + 1) | 4.14 | | | | | | |
| H2″($i$ + 1) | > | | | | | | |
| H1′($i$ + 1) | 4.92 | | | | | | |

*Note.* > represents that the distance between the two protons is larger than 5 Å. X indicates the same proton in the table.

[a] For linewidth calculations, a 4-Å distance was used based on examination of the H1′-to-H5′ region of NOESY spectra that do not support the existence of a 1.8-Å distance.

quality of selective excitation for each region of the spectrum as described in Table 2 that can be achieved using a double pulsed field gradient spin echo (DPFGSE) technique. The performance of selective time-shared homonuclear decoupling during acquisition is illustrated in Fig. 6. Figure 6A shows decoupling of the H3′ region as required for observation of the H2′/H2″ region when measuring $^3J_{H1'-H2'}$. The expanded region shows the effect of decoupling on the 1D spectrum in the H2′/H2″ region. Figure 6B illustrates the effect of H1′ decoupling required for measurement of $^3J_{H2'-H3'}$, and Fig. 6C shows the effect of decoupling the H2′/H2″ region used for measurement of the $^3J_{H3'-H4'}$. The effect of selective decoupling on individual cross peaks in two-dimensional spectra can be seen by inspection of Figs. 8–11 and will be discussed later. The use of heteronuclear $^{31}$P decoupling during acquisition can also be used to eliminate the passive coupling between the H3′ proton and the phosphorous atom, which leads to a further increase in the signal intensity as shown in Fig. 11.

*(3) J doubling.* The third approach is to apply post-acquisition data processing using the *J*-doubling method to measure antiphase peak separations in poorly resolved cross peaks. McIntyre and Freeman (*15*) have shown that the directly measured peak separation in either inphase or antiphase cross peaks is dependent on the ratio of the linewidth to the peak separation. However, peak separations measured by the *J* doubling method are relatively insensitive to the linewidth-to-peak separation, as long as the intrinsic resolution is sufficient to distinguish two peaks. Figure 7 illustrates how *J*-doubling can be used to measure the $^3J_{H1'-H2'}$ directly from the splitting of the antiphase quartet H1′-to-H2′ cross peak of A5 after all passive couplings have been collapsed. As illustrated here, *J* doubling is sensitive down to 0.1-Hz variations in the trial *J* value. The optimal *J* value is selected by determining which *J*-doubled spectrum contains the smallest residual, uncanceled signal in between the outer components. In Fig. 7, this condition is met for a trial *J* value of 9.6 Hz, whereas the residual uncanceled signal increases noticeably as the trial *J* values deviates from 9.6 Hz. This indicates that for macromolecules of this size, *J* values can be determined and reported with an accuracy of 0.1 Hz.

### *Measurement of $^3J_{H1'-H2'}$*

Optimal measurement of the $^3J_{H1'-H2'}$ required selective excitation of the H1′ region and detection of the H2′ region while selectively decoupling the H3′ region. Figure 8 compares traces taken from the H1′–H2′ cross peak of A5 taken from four different experiments. Figure 8A shows a section taken from a Stripe-COSY collected using the fully protonated oligonucleotide. A trace taken through the lowest frequency A5 cross-peak component is shown in Fig. 8E. Upon replacement of the A5 H2″ proton with a deuteron, the A5 H1′–H2″ cross peak (Figs. 8B and 8F) disappears as expected, and the A5 H1′–H2′ cross-peak intensity increases significantly, consistent with the prediction of ~50% increase in the polarization transfer (Figs. 4A and 4B) during $t_1$ and a ~75% reduction in H2′ linewidth (Figs. 3A and 3B) operative during the $t_2$ acquisition period. From inspection of Figs. 3 and 4, no further improvement is expected for exchange of the H8 proton. Further improvements can be realized by selectively decoupling the H3′ region during acquisition in the Superstripe-COSY experiment shown in Figs. 8C and 8G. The collapse of the visually apparent splittings, due to the passive couplings between the H2′ and H3′ spins, leads to an additional improvement in signal intensity. Finally, due to the H2″ to D2″ replacement and selective H3′ decoupling during acquisition, the H1′ and H2′ become effectively an isolated two-spin system. Consequently, there is no longer a requirement to use the low-sensitivity 35° pulse normally used in the P.E.COSY-type experiments. Figures 8D and 8H illustrate the significant signal enhancement obtained by application of a 90° mixing pulse. The potential improvement by using the combination of these techniques can be deduced by comparison of the traces shown in Fig. 8E to those in Fig. 8H.

The significance of this approach is further illustrated by considering the impact on the quality of spectra obtained at low

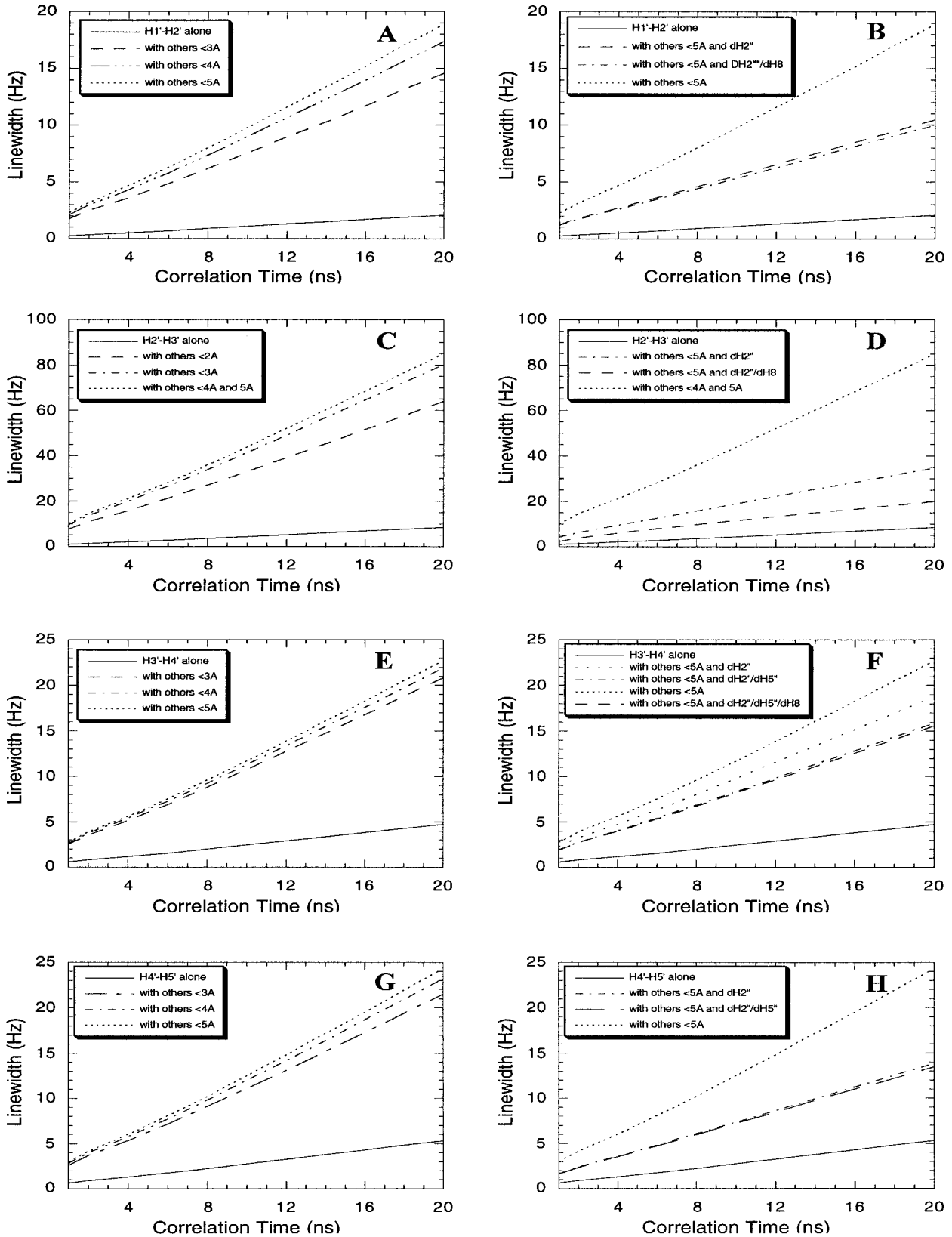


**FIG. 3.** Calculated proton linewidths for (A, B) H1′, (C, D) H2′, (E, F) H3′, and (G, H) H4′ spins. Plots on the left show linewidths calculated including all protons as a function of distance from the spin whose linewidth is considered as described in the legends. Plots on the right show calculated linewidths considering various selective deuteration patterns.

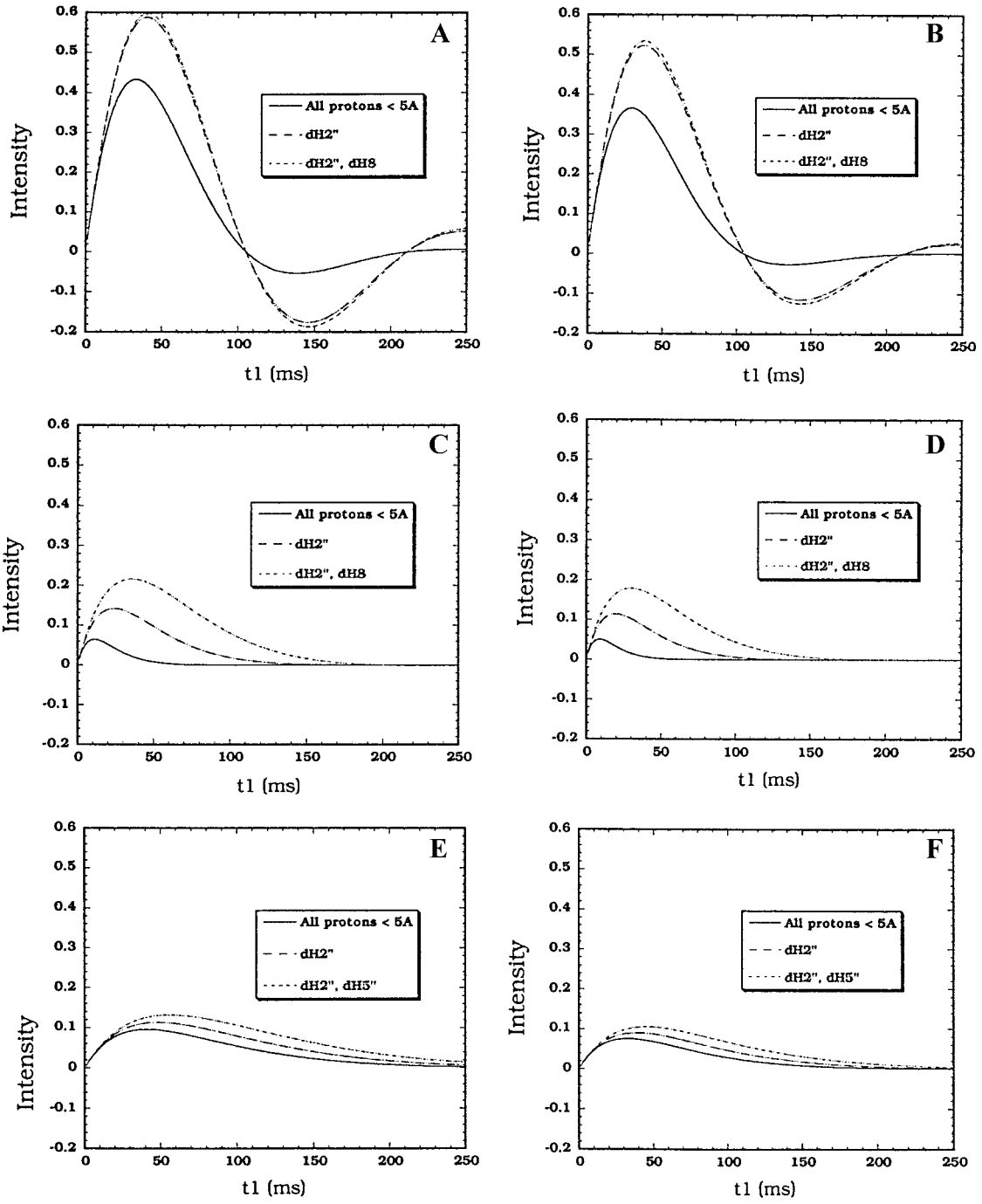


**FIG. 4.** Polarization transfer functions calculated for (A, B) H1′, (C, D) H2′, and (E, F) H3′ spins. Curves on the left are for $t_c = 6$ ns. Curves on the right are for $t_c = 8$ ns.

temperatures. Figure 9 compares the signal intensity of the A5 H1′–H2′ cross peak for protonated and deuterated samples both at 35 and at 15°C. While the signal intensity for the deuterated sample at 15°C (Fig. 9B) is only about 1/3 the intensity observed at 35°C (Fig. 9A), it is equal to the intensity of the cross peak for the protonated sample at 35°C (Fig. 9C), whereas no signal is observable for the protonated sample at 15°C (Fig. 9D). Therefore, due to the effects of broadlines and self-cancelation alone, reliable coupling constant information cannot usually be obtained at low temperatures for protonated samples. Furthermore, at low temperatures, and corresponding larger correlation times, transverse cross-relaxation effects become significant and probably can no longer be neglected in protonated samples.

**TABLE 2**
**Selective Excitation and Selective Decoupling Combinations Used for Coupling Constant Measurements**

| Coupling constant | Exc. regions | Obs. regions | Dec. regions |
|---|---|---|---|
| $J_{H1'-H2'}$ | H1′ | H2′ | H3′ |
| $J_{H2'-H3'}$ | H3′ | H2′ | H1′ |
| $J_{H3'-H4'}$ | H4′ | H3′ | H2′ |

*Measurement of* $^3J_{H2'-H3'}$

Optimal measurement of the $^3J_{H2'-H3'}$ coupling constant required selective excitation of the H3′ region and selective time-shared decoupling of the H1′ region while observing the H2′ region. Figure 10 shows results of four different experiments used for measuring $^3J_{H2'-H3'}$, all of which were collected using a 90° mixing pulse. Figure 10A shows traces of the A5 and A6 cross peaks taken from the spectrum of the fully protonated sequence. Figure 10B illustrates the improvement upon deuteration at the H2″ site. The reduced linewidth of the H3′ due to H2″-to-D2″ replacement (Figs. 3E and 3F) leads to an enhanced polarization transfer of ~30–40% during $t_1$ (Figs. 4C and 4D), while the H2′ linewidth sharpens by ~50% (Figs. 3C and 3D). The H2′ resonance experiences a large, resolved splitting due to passive coupling with the H1′ proton. Figure 10C shows the significant improvement in signal intensity resulting from selective time-shared decoupling of the H1′ region during acquisition resulting from the collapse of the ~9–10 Hz passive coupling between the H1′ and H2′ spins. Finally, because of the proximity of the H2′ spin to the H8 spin (Table 1), selective exchange of the H8 proton leads to a further reduction in the H2′ linewidth of ~50% (Fig. 3D) and a 10–20% improvement in polarization transfer (Figs. 4E and 4F) due to a somewhat longer $T_2$ of H3′. Figure 10D shows the effect of exchange of the H8 proton with a deuteron. As predicted, the enhancement of signal intensity in comparison to that shown in Fig. 10C approaches a factor of 2, an improvement due solely to the selective exchange of the H8 proton for a deuteron.

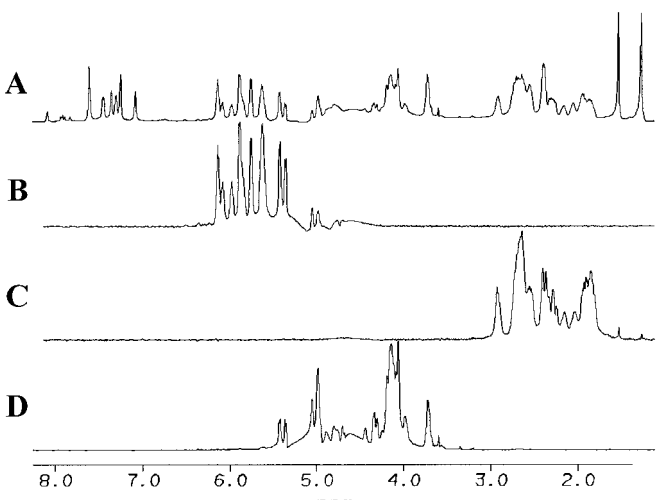


**FIG. 5.** One-dimensional 500-MHz spectra of the protonated Dickerson sample for (A) the entire proton spectrum, (B) selective excitation of the H1′ region, (C) selective excitation of the H2′ region, (D) selective excitation of the H3′/ H4′region.

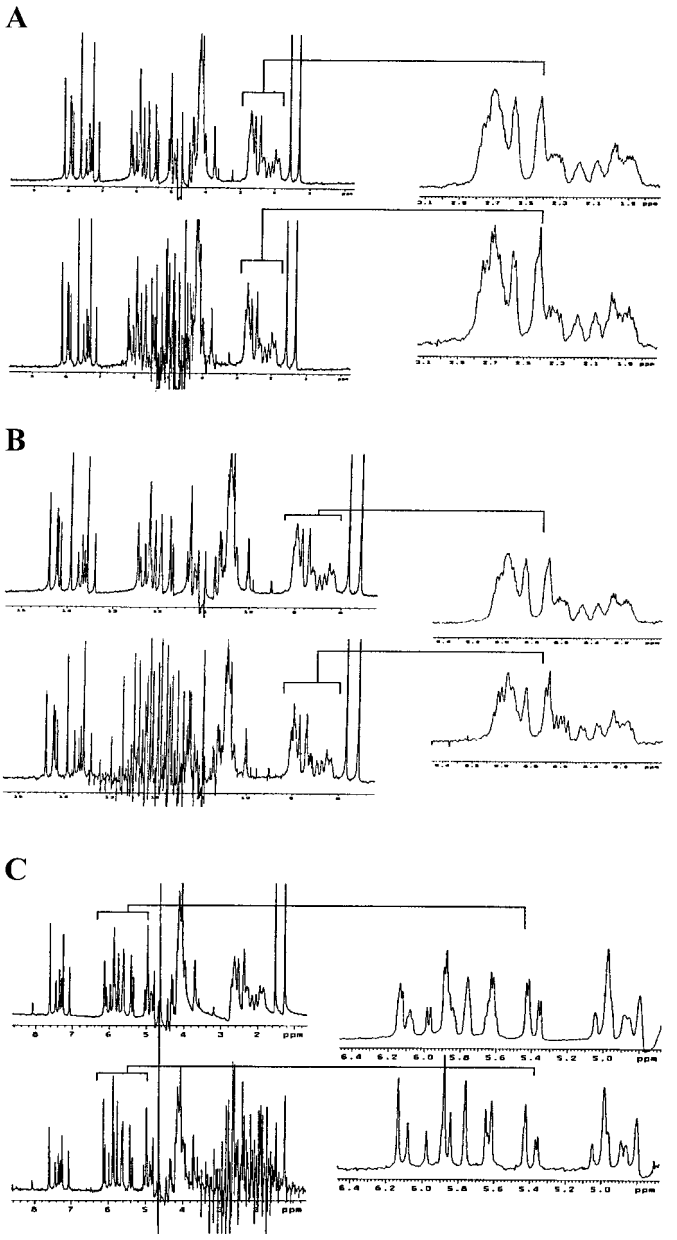


**FIG. 6.** Illustration of the performance of selective time-shared decoupling of (A) the H3′ region, (B) the H1′ region, and (C) the H2′ region. Spectra on the left show the coupled (top) and decoupled (bottom) spectra. Scrambling of the spectrum is observed in the decoupled region in the bottom spectra. The insets shown at the right allow comparison of the coupled (top) and decoupled (bottom) spectrum for each region being detected.

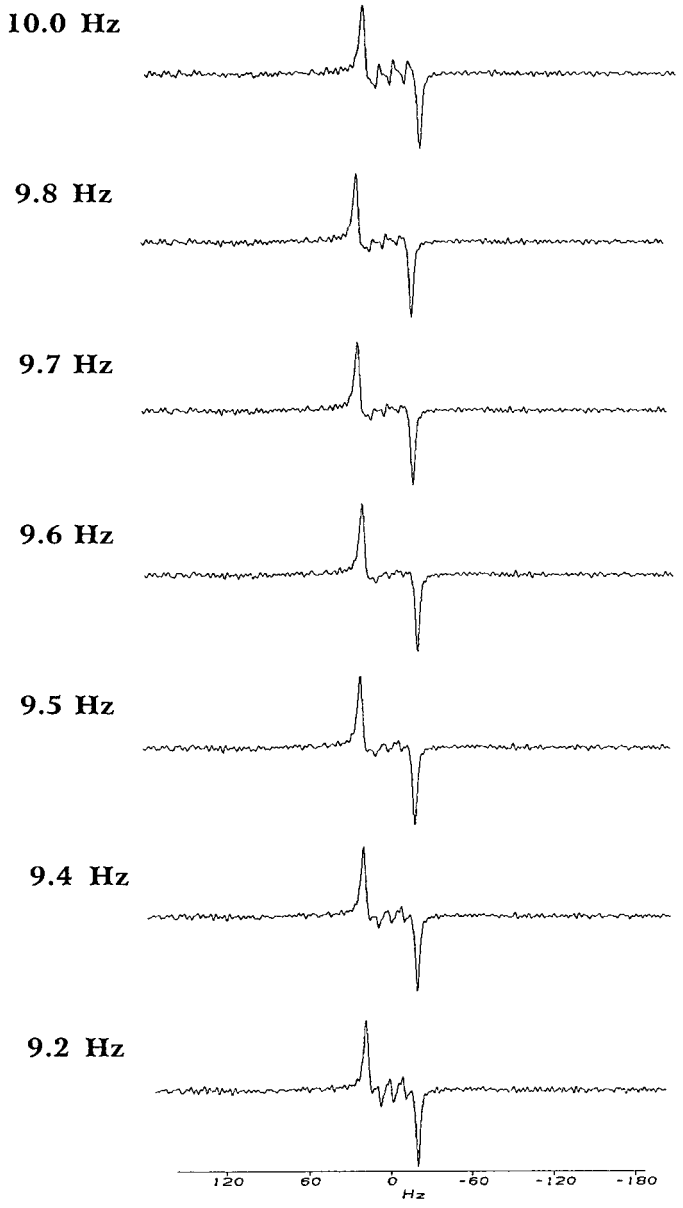


**FIG. 7.** Traces taken from the H1′–H2′ cross peak in the H2″ deuterated sample following *J*-doubling post-data acquisition processing. The trial *J* value is shown in the upper left-hand corner for each spectrum.

### *Measurement of $^3J_{H3'-H4'}$*

The measurement of $^3J_{H3'-H4'}$ coupling constants remains challenging because the cross peaks occur close to the diagonal of the 2D spectrum and are often difficult to resolve. Furthermore, in B-form DNA the vicinal $^3J_{H3'-H4'}$ coupling constant is quite small at ~3 Hz and, as shown in Figs. 4E and 4F, only ~10–15% of the potential magnetization is expected to be converted to observable antiphase magnetization at the time of the mixing pulse. This results in inherently low-intensity cross peaks. Unfortunately, the H4′ proton is located ~4 Å or greater from the H2″ and H8 protons (Table 1). Consequently, no significant effect on the H4′ linewidth is observable with the H2″-to-D″ or H8-to-D8 replacement. However, the H4′ spin is close to the both the H5′ and H5″ spins. Therefore, replacement of one or both H5′ protons with a deuteron should have a significant line-narrowing effect (as shown in Figs. 3G and 3H). To resolve the cross peaks close to the diagonal, a Stripe-DQF-COSY was used instead of Stripe-COSY. Selective excitation was applied to the narrow region shown in Fig. 5D. There are two passive couplings, $^3J_{H2'-H3'}$ and $^3J_{H3'-P}$, which can potentially broaden the H3′–H4′ cross peaks along the F2 dimension due to unresolved splittings. Selective time-shared homonuclear decoupling was applied to the H2′/H2″ region to collapse the H2′–H3′ passive couplings during acquisition, and the expected increase in signal intensity for the H3′–H4′ cross peaks is illustrated in Figs. 11A and 11B. The signal enhancement due to heteronuclear $^{31}$P decoupling on a DQF-COSY is shown in Figs. 11C and 11D.

### *Summary of Coupling Constant Measurements*

The coupling constants, $^3J_{H1'-H2'}$, $^3J_{H2'-H3'}$, and $^3J_{H3'-H4'}$, were determined by measuring the splitting of antiphase components, by *J*-doubling analysis, or by measurement of the displacement of cross peaks by passive couplings. A summary of all measurements is listed in Tables 3–5. The cross peaks for the A5 and A6 residues enable evaluation of the effect of selective deuteration on each type of coupling constant. Inspection of the $^3J_{H1'-H2'}$ values summarized in Table 3 indicate that overall the *J* values do not vary significantly; i.e., all agree within ±0.3 Hz, depending on what method of measurement was used, and compare well with the values reported by Bax and Lerner (*17*). A slightly smaller variation of ±0.2 Hz was observed for the A5 and A6 residues. It is worthwhile to note that the values obtained here required no special processing of the data to compensate for linewidth-dependent splittings, except for in the case of *J* doubling. The collection of high-sensitivity data combined with selective decoupling of the passive H1′ appears sufficient to allow accurate measurement of $^3J_{H1'-H2'}$, even in the protonated samples. Since selective deuteration reduces the magnitude of transverse cross relaxation by about 42-fold, the observation of no significant change for $^3J_{H1'-H2'}$ upon deuteration indicates that for DNA oligonucleotides of this length and at 35°C, the effects of transverse cross relaxation are negligible. Therefore, transverse cross-relaxation effects cannot be used to explain deviations of the A5 and A6 sugar conformations by up to 7° from pure south.

In Table 4, the same general observation derived for the $^3J_{H1'-H2'}$ can be made about the $^3J_{H1'-H2''}$ values. Thymidine residues seem to be an exception, as values taken from the protonated sample or from direct measurement of the splittings of the antiphase cross peaks are larger than the concensus from other methods, and appear to reflect the artifacts due to self-cancelation. This probably stems from broader resonance lines due to the high proton density involving the C5 methyl and H6

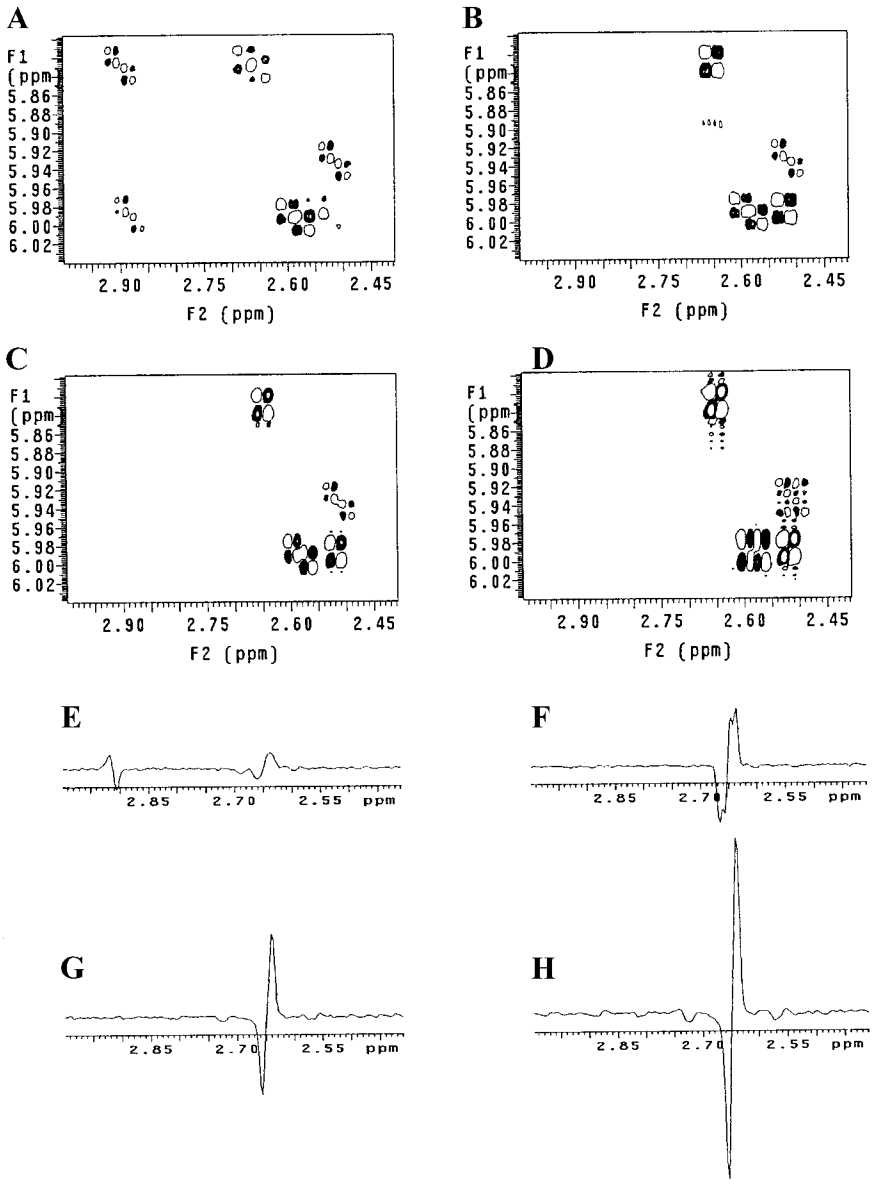


**FIG. 8.** Illustration of progressive improvement in signal-to-noise ratio of the A5 H1′–H2′ cross peak as strategic steps are applied sequentially. (A) Contour plot of the Stripe-COSY spectrum for the protonated sample in the H1′-to-H2′/H2″ region of the spectrum. (B) Contour plot of the Stripe-COSY spectrum for the A5, A6 *d*H2″ sample in the H1′-to-H2′/H2″ region of the spectrum. (C) Contour plot of the Stripe-COSY spectrum for the A5, A6 *d*H2″ sample in the H1′-to-H2′/H2″ region of the spectrum collected using selective time-shared H3′ decoupling during acquisition. (D) Contour plot of the Stripe-COSY spectrum for the A5, A6 *d*H2″ sample in the H1′-to-H2′/H2″ region of the spectrum collected using a 90° mixing pulse and selective time-shared H3′ decoupling during acquisition. (E) Trace taken through the A5 cross peak shown in (A). (F) Trace taken through the A5 cross peak shown in (B). (G) Trace taken through the A5 cross peak shown in (C). (H) Trace taken through the A5 cross peak shown in (D).

proton. Finally, Table 5 summarizes the observed $^3J_{H2'-H3'}$ and $^3J_{H3'-H4'}$ values. Overall, we find values for $^3J_{H2'-H3'}$ appear systematically smaller that those reported by Bax and Lerner (*17*). However, it is not possible to do a complete comparison since 4 of the 12 cross peaks were overlapped in our spectra and we report a comparable value for only the C9 residue. For the most part, the values measured here agree with those reported by Bax and Lerner. One notable exception is the value reported for the A5 where Bax and Lerner reported a value of 2.5 Hz and we determined a value of 3.4 Hz. Based on the relative weak intensity of the G2, G4, and G10 cross peaks compared to those observed for the A5 and A6 cross peaks, one might expect the couplings to be distinctly larger for the A5 and A6 residues. Using the J doubling technique, we determined a value of 3.4 Hz, more consistent with the pattern of relative cross-peak intensities (Fig. 12). Here, the values reflect selective decoupling of passive spins during the acquisition period, and no special data processing was applied in the

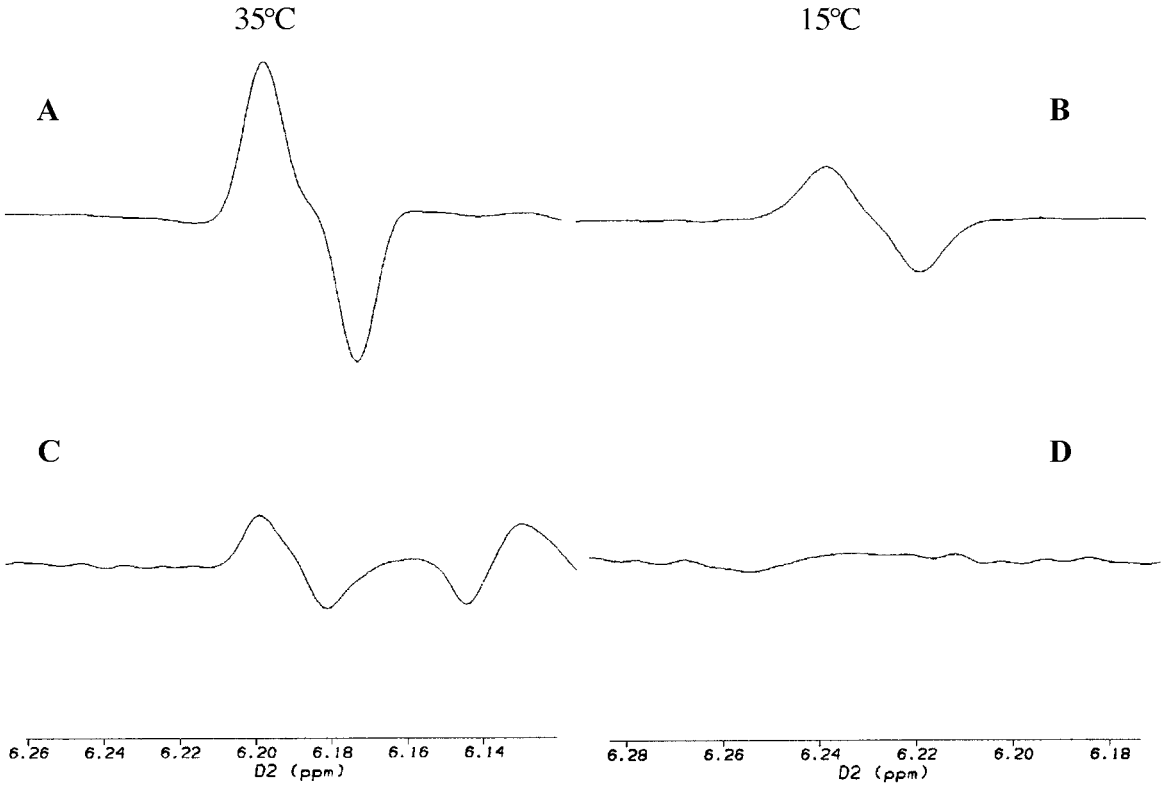


**FIG. 9.** Traces taken through the A6 H1′–H2′ cross peak for the deuterated sample (A) at 35°C and (B) at 15°C and for the protonated sample at (C) 35°C and (D) at 15°C.

analysis of the $^{3}J_{H3'-H4'}$ as used in the data analysis reported by Bax and Lerner (*17*).

## CONCLUSIONS

The coupling constant data reported here, for the most part, are consistent with those reported by Bax and Lerner (*17*) with the largest deviations occurring in the case of very small coupling constants such as the H3′–H4′ class. The H1′–H2′ data support the prior conclusion concerning the population distribution of conformers at the A5 and A6 positions in the sequence, i.e., 94% South with 6% North. Consequently, the 6–7% deviation from S conformation cannot be due to the effects of transverse cross relaxation. Other factors such as additional motion and pucker angle variations should still be considered. While no considerable change in the coupling constants was observed for the A5 and A6 residues upon stereo-selective deuteration, these results indicate that for dodecamers at 35°C, the consequences of transverse cross relaxation are negligible. However, for larger DNA fragments and for studies at lower temperatures, the consequences of transverse cross relaxation are predicted to be significant and the strategy of stereoselective deuteration appears to be the definitive solution for eliminating the effects of transverse cross relation under those conditions. Furthermore, it will be interesting to examine if stereo-selective deuteration affects the measured values in other residues in the same sequence, especially those pyrimidines that have been interpreted as having large fractions of north population, such as T7 (15%N) and C9 (20%N).

The overall objective of improving the accuracy of vicinal coupling constants in DNA is to enable a more meaningful analysis of sugar conformations. This is especially important since many structural studies, e.g., investigation of sequence-dependent structural features and structural perturbations due to damaging agents, focus on detecting subtle changes in DNA structure. The strategy outlined here provides a means of improving the accuracy with which very small coupling constants can be measured by virtue of the increased sensitivity of the overall approach. For larger coupling constants, it appears all methods provide precise and accurate measurements, albeit the approach outlined here enables the same quality data to be obtained in a much shorter period of spectrometer time. Given accurate and precise coupling constant data, the usual practice is to interpret the coupling constant data in terms of fitting the data to an optimized Karplus relationship, and the data are further fitted by allowing for the sugar ring to undergo a dynamic puckering between north and south conformations. The latter practice raises the question as to whether the inabil-

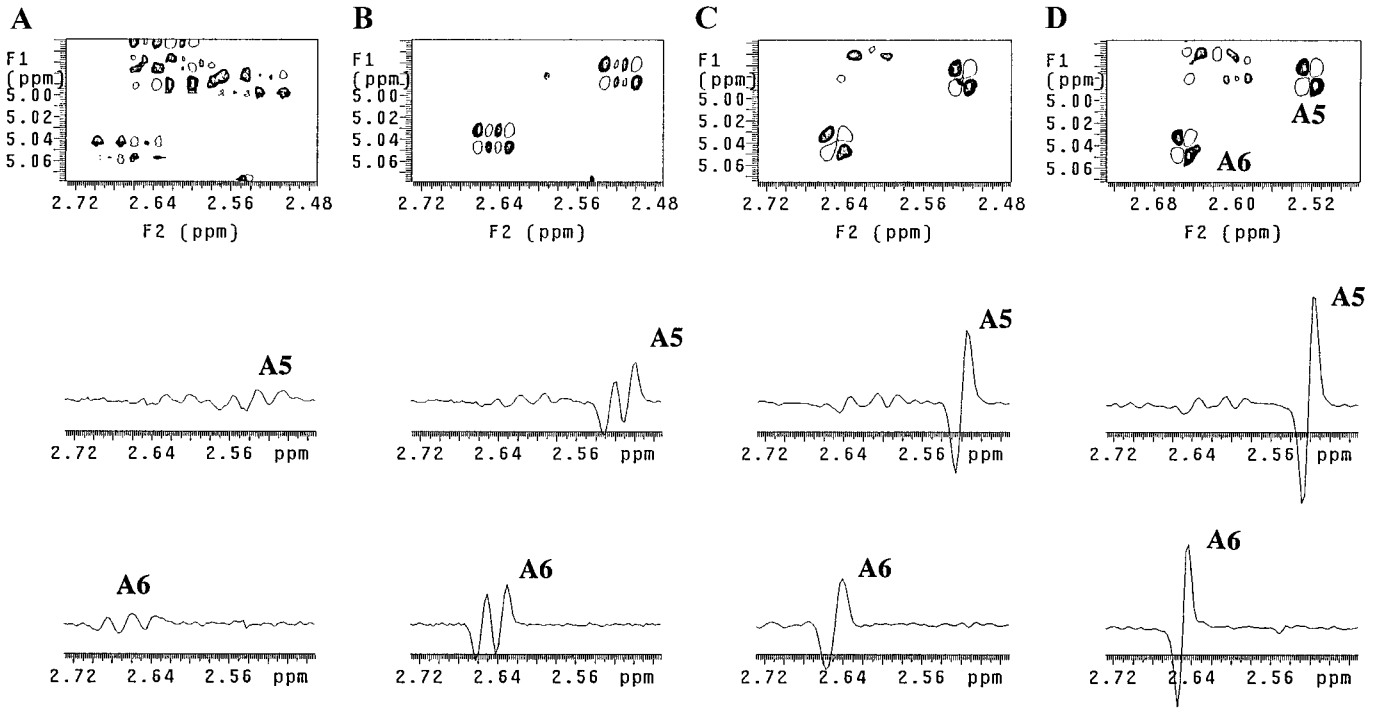


**FIG. 10.** Illustration of progressive improvement in signal-to-noise ratio of the A5 H2′–H3′ cross peak as strategic steps are applied sequentially. (A) Contour plot of the Stripe-COSY spectrum for the protonated sample in the H2′-to-H3′ region of the spectrum. (B) Contour plot of the Stripe-COSY spectrum for the A5, A6 *d*H2″ sample in the H2′-to-H3′ region of the spectrum. (C) Contour plot of the Stripe-COSY spectrum for the A5, A6 *d*H2″ sample in the H2′-to-H3′ region of the spectrum using selective time-shared H1′ decoupling during acquisition. (D) Contour plot of the Stripe-COSY spectrum for the A5, A6 *d*H2″ and *d*H8 samples in the H2′-to-H3′ region of the spectrum using selective time-shared H1′ decoupling during acquisition. Traces shown below are taken from the A5 and A6 cross peaks, respectively.

ity to fit the data to a Karplus relationship in the absence of dynamics is due to an imperfect optimization for the coefficients in the Karplus equation, e.g., for all sequence contexts, or whether the dynamics is actually occurring. It is somewhat disconcerting that a dynamic model is widely, automatically applied even in the absence of direct experimental evidence of sugar ring interconversion between north and south conformers. So, at this time, it would appear that the limiting factor in obtaining meaningful sugar conformation analysis in DNA is the precision, or lack thereof, with which the current generation of optimized Karplus coefficients can predict the value of the vicinal coupling constants as a function of the pseudorotation angle.

In conclusion, a comprehensive approach is proposed for collecting coupling constant data required for a complete analysis of the sugar conformations in DNA. Striking improvements in both sensitivity and resolution can be obtained by means of stereo-selective deuterium replacement, selective excitation, and selective decoupling during acquisition. These methods do not rely on raising the temperature of the sample, which can lead to changes in the structure of the DNA. In fact, stereo-specific deuteration allows high-quality coupling constant data to be collected even at very low temperatures $\leq 5°C$, data that is virtually impossible to collect using nondeuterated samples. This approach is therefore powerful for characterization of very labile DNA molecules that contain structure-disrupting lesions that require spectroscopic studies at very low temperatures in order to prevent DNA melting. Furthermore, because of the dramatic overall increase in sensitivity and resolution by the approaches outlined here, the strategy represents an enabling technique for characterizing the structure of large nucleotide fragments and for DNA and RNA fragments bound to proteins. The implementation of stereo-selective deuterium replacement requires the synthesis of selectively labeled phosphoramidites. We are currently developing the chemistry to produce optimal labeling patterns for all nucleotides of interest. Finally, the selective excitation and decoupling applications are relatively straightforward to implement with current generations of NMR spectrometers.

## EXPERIMENTAL

*Synthesis of DNA oligonucleotides.* Both the Dickerson sequence (5′-CGCGAATTCGCG-3′) and the deuterated Dickerson sequence (5′-CGCG$^{d}$A$^{d}$ATTCGCG-3′) were prepared on an Applied Biosystems DNA/RNA Synthesizer, Model 392. All reagents were obtained from Applied Biosystems, with the exception of Optima-grade acetonitrile and HPLC-grade di-

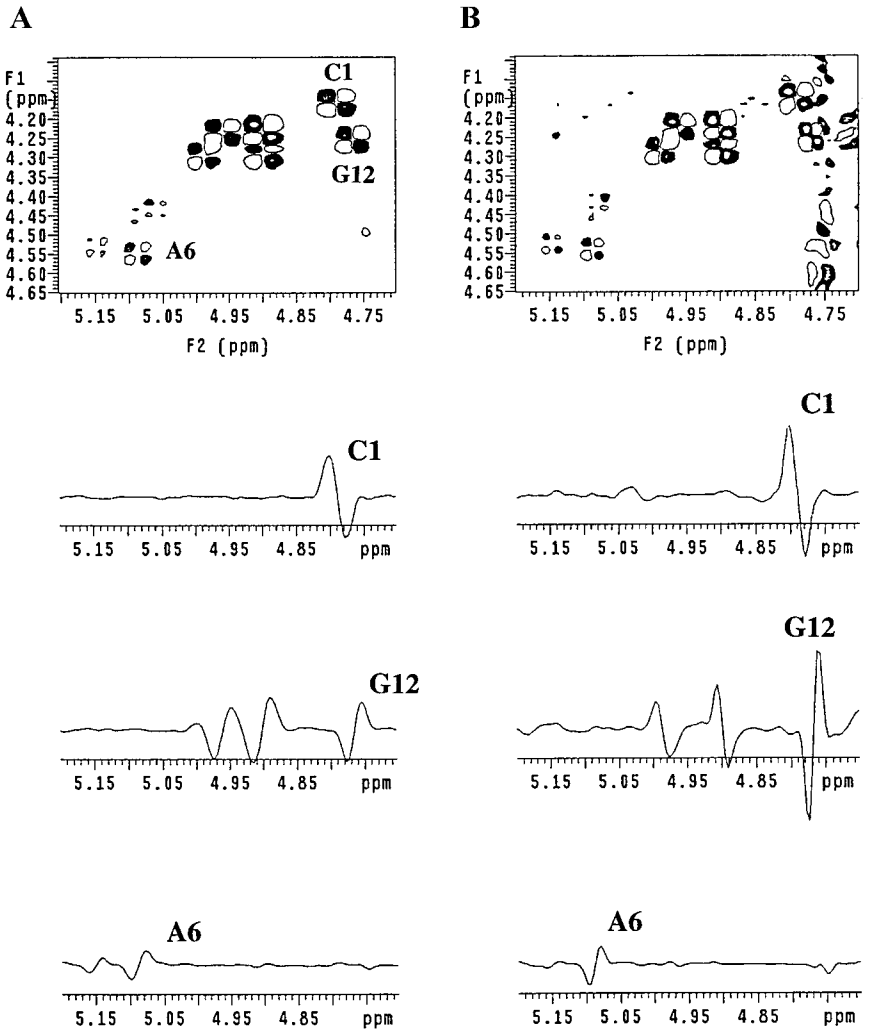


**FIG. 11.** Illustration of progressive improvement in signal-to-noise ratio of the H3′–H4′ cross peaks (A) Contour plot of the DQF-COSY spectrum for the protonated sample in the H3′-to-H4′ region of the spectrum. (B) Contour plot of the DQF-COSY spectrum for the A5, A6 *d*H2″ sample in the H3′-to-H4′ region of the spectrum using selective time-shared H2′/H2″ decoupling during acquisition. Traces shown below spectra are taken from the C1, G12, and A6 cross peaks, respectively. (C) Contour plot of the DQF-COSY spectrum for the A5, A6 *d*H2″ sample in the H3′-to-H4′ region of the spectrum. (D) Contour plot of the DQF-COSY spectrum for the A5, A6 *d*H2″ sample in the H3′-to-H4′ region of the spectrum heteronuclear $^{31}$P decoupling during acquisition. Traces shown below are taken from the C9 and A5 cross peaks, respectively.

chloromethane, which were obtained from Fisher, and the deuterated adenine base was prepared as described elsewhere (*8*). Each oligo synthesis was 10 $\mu$M in scale, and detritylation was performed on the support column as a part of the synthesis procedure. The crude oligo mixtures were then deprotected in ammonium hydroxide overnight (15 h) at 55°C. Subsequent to deprotection, the samples were dried overnight in a Labconco Centrivap Concentrator, and stored frozen at −20°C until purification.

*Sample purification.* Crude oligo mixtures were purified on a Waters PrepLC 4000 system, using a reverse phase Delta-Pak C18 15-$\mu$m column. Each sample was dissolved in 1 mL of loading buffer (0.1 M triethylamine, 5% acetonitrile, adjusted to pH 6.5 with acetic acid) and vortexed to mix, then filtered through a 0.45 $\mu$M syringe filter into a clean Eppendorf tube. Injection volumes were 250 $\mu$L each. The eluting buffer was pure acetonitrile. The method of elution employed a 0−8% gradient of eluting buffer, followed by a column-washing gradient from 8−40% acetonitrile. Fractions were collected using a Pharmacia LKB SuperFrac, and fractions containing the desired oligomer were combined and dried on the Centrivap concentrator.

Dried samples were redissolved in 600 $\mu$L each of deionized water (Millipore MilliQ system). One-dimensional NMR survey spectra showed the samples to be contaminated with residual triethylamine believed to be bound to the phosphate groups of the DNA. The triethylamine was removed by flow dialysis overnight against against 100 mM phosphate buffer,

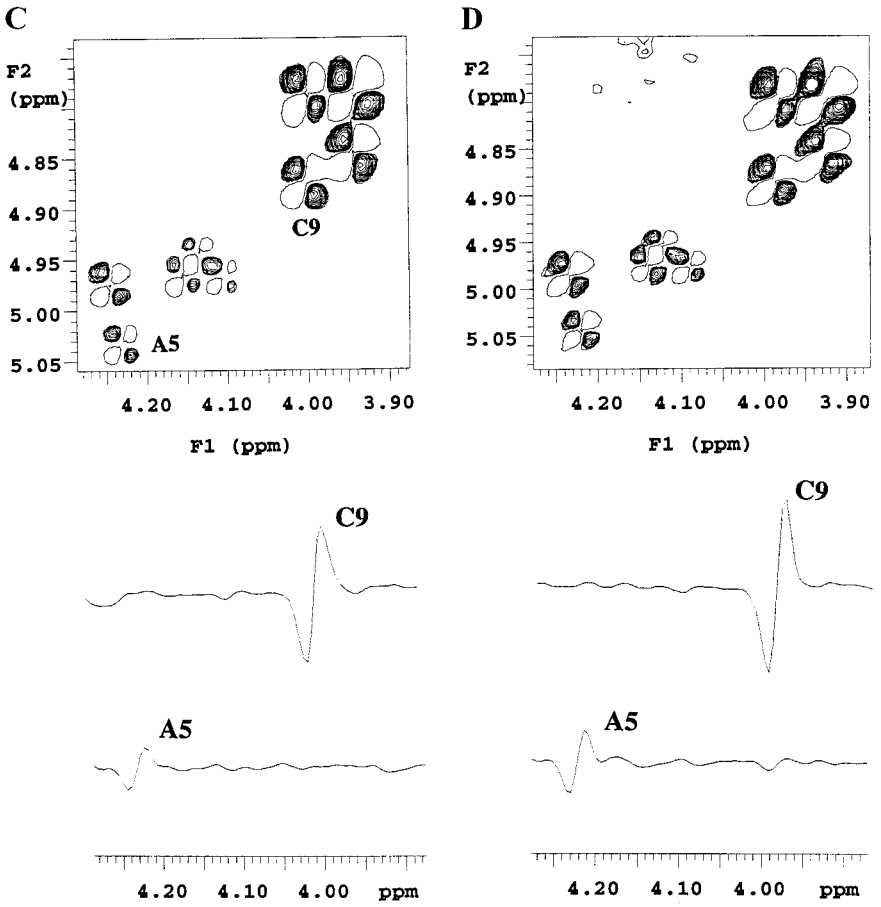


**FIG. 11**—*Continued*

pH 7, using a Rabbit peristaltic pump at 1 mL/min flow rate. Subsequent NMR spectra showed this method successfully removed triethylamine. The samples were then dialyzed according to the same method against 20 mM phosphate, 200 mM sodium chloride at pH 7. The dialyzed samples were lyophilized overnight on a Flexidry MP lyophilizer, and redissolved in 600 $\mu$L each of 99.96% deuterium oxide (Cambridge Isotopes, Inc.) to give the final NMR samples.

*Exchange of purine H8 protons.* In order to allow exchange of labile protons for deuterons, the sample pH of both the Dickerson sequence and the deuterated Dickerson sequence were adjusted to 8 using sodium deuteroxide. The samples were then incubated for two days at 75°C, after which the exchange reaction was judged to be complete based on inspection of one-dimensional NMR spectra. The pH of both samples was then adjusted back to 7 using deuterium chloride.

*NMR spectroscopy.* All NMR experiments were performed on Varian UNITY*plus* 500-MHz or 750-MHz spectrometers equipped with a radiofrequency waveform generator unit. All selective excitation pulses and selective decoupling pulses were generated using the Pbox program within the VNMR 5.1 software. The homonuclear selective decoupling during the acquisition was implemented using a time-shared decoupling pattern on the $^1$H channel. All NMR spectra were recorded in $D_2O$ at 35°C.

*Time-shared homonuclear decoupling.* The time-shared homonuclear decoupling scheme was executed in the Varian pulse sequence by using a hard-loop coded into the pulse sequence so that during the dwell time between points, the proton decoupler is turned on, using a shaped, selective decoupling sequence, for a fraction of the dwell time, and then the receiver is turned on for the remainder of the dwell period. The fraction of time the decoupler is turned on can be described as a duty cycle. Duty cycles of 15–20% are usually sufficient to generate decoupling, with a corresponding 15–20% sacrifice in signal while the decoupler is turned on during the dwell period.

The DQF-COSY experiment was acquired as a 1024 $\times$ 512 complex matrix with a spectral width of 4000 Hz in both F2 and F1, corresponding to acquisition times of 0.256 and 0.128 s, respectively. A total of 32 scans was acquired per FID with a repetition delay of 2.0 s. The data were apodized in F2 and F1 using 75° and 65° shifted sine-bell with 0.1 and 0.06 as constants in Gaussian functions respectively, and were subse-

**TABLE 3**
**Summary of $^3J_{H1'-H2'}$ Coupling Constant Measurements**

| | A | B | C | D | E |
|---|---|---|---|---|---|
| C1 | 7.9 | 8.0 | 7.8 | 7.9 | 8.2 |
| G2 | 9.8 | 9.6 | 9.5 | 9.7 | 10.1 |
| C3 | 8.9 | 9.3 | 8.8 | 8.6 | 8.8 |
| G4 | 10.1 | 10.0 | 9.9 | 9.8 | 10.2 |
| A5 | 9.8 | 9.7 | 9.6 | 10.0 | 9.7 |
| A6 | 9.7 | 9.4 | 9.4 | 9.5 | 9.3 |
| T7 | 8.7 | 8.9 | 8.2 | 8.5 | 8.5 |
| T8 | 10.0 | 9.3 | 10.2 | 9.8 | 9.5 |
| C9 | 8.9 | 8.9 | 8.8 | 9.0 | 8.7 |
| G10 | 10.2 | 10.1 | 9.8 | 9.5 | 9.7 |
| C11 | 8.4 | 8.4 | 7.8 | 8.5 | 8.4 |
| G12 | 7.9 | 8.0 | 7.9 | 7.6 | 8.1 |

*Note.* A: From fully protonated Dickerson sequence taken from direct measurement of separation of the minima and maxima of the antiphase doublet components. The average standard deviation was 0.21 Hz. B: From A5–*d*H2″, A6–*d*H2″ selectively deuterated Dickerson sequence taken from direct measurement of separation of the minima and maxima of the antiphase doublet components. The average standard deviation was 0.18 Hz. C: From A5–*d*H2″, A6–*d*H2″ selectively deuterated Dickerson sequence taken from *J*-doubling analysis of separation of the minima and maxima of the antiphase doublet components. The average standard deviation was 0.10 Hz. D: From A5–*d*H2″, A6–*d*H2″ selectively deuterated Dickerson sequence taken from measurement of displacement of peaks by passive couplings. The average standard deviation was 0.21 Hz. E: From Table 1 of Bax and Lerner (*17*).

**TABLE 4**
**Summary of $^3J_{H1'-H2''}$ Coupling Constant Measurements**

| | A | B | C | D | E |
|---|---|---|---|---|---|
| C1 | 5.9 | 6.0 | 6.0 | 6.6 | 6.1 |
| G2 | 6.3 | 6.8 | 5.3 | 5.4 | 5.7 |
| C3 | 5.8 | 5.9 | 5.2 | 6.1 | 6.2 |
| G4 | 5.6 | 6.0 | 5.2 | 5.4 | 5.1 |
| A5 | 6.5 | | | | 5.7 |
| A6 | 6.2 | | | | 6.0 |
| T7 | 7.4 | 7.2 | 5.4 | 6.1 | 6.2 |
| T8 | 7.0 | 6.8 | 6.5 | 5.7 | 6.0 |
| C9 | 5.7 | 5.7 | 5.1 | 5.9 | 6.0 |
| G10 | 6.4 | 6.6 | 5.2 | 5.6 | 5.5 |
| C11 | 6.4 | 6.0 | 6.1 | 6.9 | 6.2 |
| G12 | 6.4 | 6.3 | 6.2 | 6.2 | 6.3 |

*Note.* A: From fully protonated Dickerson sequence taken from direct measurement of separation of the minima and maxima of the antiphase doublet components. The average standard deviation was 0.19 Hz. B: From A5–*d*H2″, A6–*d*H2″ selectively deuterated Dickerson sequence taken from direct measurement of separation of the minima and maxima of the antiphase doublet components. The average standard deviation was 0.31 Hz. C: From A5–*d*H2″, A6–*d*H2″ selectively deuterated Dickerson sequence taken from *J*-doubling analysis of separation of the minima and maxima of the antiphase doublet components. The average standard deviation was 0.10 Hz. D: From A5–*d*H2″, A6–*d*H2″ selectively deuterated Dickerson sequence taken from measurement of displacement of peaks by passive couplings. The average standard deviation was 0.34 Hz. E: From Table 1 of Bax and Lerner (*17*).

quently zero filled to twice the size, followed by a Fourier transformation.

The selective DQF-COSY experiment was acquired as a 1024 × 240 complex matrix with a spectral width of 3499 Hz in F2 and 1900 Hz in F1, corresponding to acquisition times of 0.293 and 0.126 s, respectively. A total of 64 scans were acquired per FID, with a repetition delay of 2.0 s. A 3.2-ms e-BURP pulse with a 722-Hz field was used to selectively excite the H3′/H4′/H5′ region, and a e-BURP pulse with a 1441-Hz field was used to selectively decouple the H2′/H2″ region. The data were apodized in F2 and F1 using 65° and 80° shifted sine-bell functions, respectively, and with 0.06 Gaussian constants in both cases, and were subsequently zero filled to 4096 points in F2 and 1024 points in F1, followed by a Fourier transformation.

The Stripe-COSY experiment for observing the H1′–H2′/H2″ region was acquired as a 1024 × 70 complex matrix with a spectral width of 3000 Hz in F2 and 500 Hz in F1, corresponding to acquisition times of 0.341 and 0.140 s, respectively. A total of 96 scans were acquired per FID, with a repetition delay of 2.0 s. A 7.7-ms e-BURP pulse with a 322-Hz field was used to selectively excite the H1′ region, and a e-BURP pulse with a 1441-Hz field was used to selectively decouple the H3′ region. The data were apodized in F2 and F1 using 30° and 30° shifted sine-bell with 0.3 and 0.5 as constants in Gaussian functions respectively, and were subsequently zero filled to 4096 points in F2 and 512 points in F1, followed by Fourier transformation.

The Stripe-COSY experiment for observing the H3′–H2′/

**TABLE 5**
**Summary of $^3J_{H2'-H3'}$ and $^3J_{H3'-H4'}$ Coupling Constant Measurements**

| | $^3J_{H2'-H3'}$ | | $^3J_{H3'-H4'}$ | |
|---|---|---|---|---|
| | A | B | C | D |
| C1 | | 6.3 | | 3.3 |
| G2 | 4.5 | | 2.6 | 2.9 |
| C3 | | 6.1 | 3.8 | 3.4 |
| G4 | | | 2.9 | 2.3 |
| A5 | 5.1 | | 3.4 | 2.5 |
| A6 | 5.1 | | 3.5 | 3.0 |
| T7 | | | 3.0 | 4.7 |
| T8 | 5.7 | | 3.0 | 3.1 |
| C9 | 5.6 | 6.9 | 3.0 | 3.6 |
| G10 | | | 2.4 | 2.4 |
| C11 | | 6.6 | 2.5 | 4.0 |
| G12 | | 6.3 | | 3.2 |

*Note.* A: From A5–*d*H2″, A6–*d*H2″ selectively deuterated Dickerson sequence determined by *J*-doubling analysis of cross peaks taken from Stripe-COSY experiments. The average standard deviation was 0.19 Hz. B: From Table 1 in Lerner and Bax (*17*). C: From A5–*d*H2″, A6–*d*H2″ selectively deuterated Dickerson sequence determined by *J*-doubling analysis of antiphase cross peaks taken from Stripe-COSY experiments. The average standard deviation was 0.19 Hz. D: From Table 2 in Bax and Lerner (*17*).

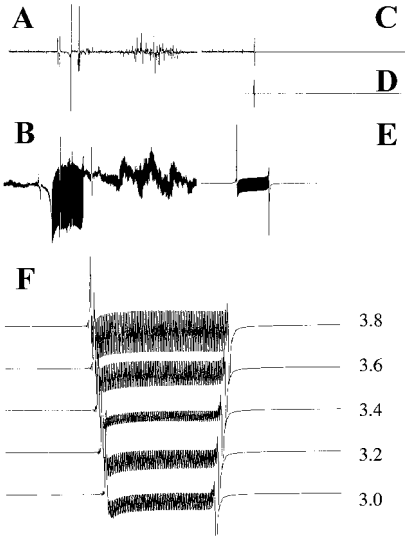


**FIG. 12.** (A) Trace taken through the A5 cross peak in the H2″deuterated sample in the H3′-to-H4′ region of the spectrum. (B) Spectrum following *J* doubling with no trapezoid apodization. (C) Trapezoid function applied to the trace through the A5 cross peak. (D) Second trapezoid function applied to the trace through the A5 cross peak after reversing the spectrum in (C). (E) Spectrum following *J* doubling of the spectrum in (D). (F) Spectra of the A5 cross peak with trial *J* values shown to the right of each spectrum. The optimal value for *J* in the A5 cross peak is 3.4 Hz.

H2″ region was acquired as a 960 × 47 complex matrix with a spectral width of 2799 Hz in F2 and 300 Hz in F1, corresponding to acquisition times of 0.343 and 0.156 s, respectively. A total of 64 scans were acquired per FID, with a repetition delay of 2.0 s. A 13.4-ms e-BURP pulse with a 162-Hz field was used to selectively excite the H3′/H4′/H5′ region, and a e-BURP pulse with a 2876-Hz field was used to selectively decouple the H1′ region. The data were apodized in F2 and F1 using 20° and 45° shifted sine-bell with 0.2 and 0.3 as constants in Gaussian fuctions respectively, and were subsequently zero filled to 4096 points in F2 and 256 points in F1, followed by Fourier transformation.

*J doubling.* The time-domain NMR signal $S(t)$ representing an antiphase cross peak is represented by the expression

$$S(t) = (1/2)\exp(-i2\pi\delta t)\exp(-\lambda t)\sin(\pi J_a t), \qquad [1]$$

where $\delta$ is the chemical shift, $\lambda = 1/T_2^*$ is the instrumental linewidth, and $J_a$ is the active coupling constant. The *J* doubling method is based on a time-domain operation in which the signal is multiplied by $\cos(\pi J^* t)$, where $J^*$ is the trial coupling constant:

$$S(t) = (1/2)\exp(-i2\pi\delta t)\exp(-\lambda t)\sin(\pi J_a t)\cos(\pi J^* t). \qquad [2]$$

Based on a well-known trigonometrical identity, this may be rewritten as

$$S(t) = (1/4)\exp(-i2\pi\delta t)\exp(-\lambda t) \times \{\sin[\pi(J^* + J_a)t + \sin[\pi(J^* - J_a)t]\}. \qquad [3]$$

The Fourier transformation of $S(t)$ produces a four-line spectrum made up of two antiphase doublets. The inner antiphase doublet with splitting $|J^* - J_a|$ vanishes when $J^* = J_a$, and the outer antiphase doublet with splitting $|J^* + J_a|$ that becomes $2J_a$ achieves a maximum intensity when $J^* = J_a$. The optimal value of $J^*$ occurs when the integral of the absolute magnitude of the inner doublet is a minimum. The traces used for the *J*-doubling analysis normally are taken from the F2 axis since it usually has a digital resolution higher than that of the F1 axis.

*Calculation of proton linewidths.* The proton linewidths were calculated according to $\mathrm{LW} = 1/(\pi T_2^*)$ where $1/T_2^* = 1/T_2 + 1/T_2(\mathrm{inhom})$. If the $T_2(\mathrm{inhom})$ is ignored, the linewidth is equal to $1/T_2 = R_2$. For a pair of isolated proton spins with intramolecular, dipole–dipole interactions, the transverse relaxation rate ($R_2$) of the proton magnetization is expressed as (*18*)

$$R_2 = (3/40)(2\pi D)^2[3J(0) + 5J(\omega_0) + 2J(2\omega_0)], \qquad [4]$$

where $J(\omega) = 2\tau_c/(1 + \omega^2\tau_c^2)$, $D = (\mu_0/4\pi)h\gamma_H^2 r_{AB}^{-3}$. For a multiproton spin system, the above equation is modified by replacing $r_{AB}^{-6}$ with the sum over all additional protons, $\sum_B r_{AB}^{-6}$ (assuming a single correlation time).

*Calculations of polarization transfer during $t_1$ evolution.* In all correlation experiments described, e.g., the stripe-COSY, the cross peak between spins is observable due to the accumulation of antiphase magnetization during the $t_1$ evolution period. The signal intensity is therefore proportional to a convolution of the amplitude of the antiphase magnetization with the exponential $T_2$ decay of the transverse component of the antiphase magnetization. Therefore, if one considers the H1′–H2′ cross peak where the H1′ region is selectively excited, the antiphase magnetization during $t_1$ is represented by $2I_{x,y}^{H1'} I_z^{H2'}$ with coefficients, $\sin(\pi^3 J_{H1'-H2'} t_1)$, for active coupling plus additional terms for any passive couplings. The coherence transfer efficiency has the relationship

$$\text{Coherence transfer} \propto \sin(\pi^3 J_{H1'-H2'} t_1)\exp(-t_1/T_2). \qquad [5]$$

## ACKNOWLEDGMENTS

We gratefully acknowledge the helpful discussions concerning implementation of time-shared homonuclear decoupling with Dr. Eriks Kupce. This work was performed under the auspices of the Department of Energy (Contracts DE-AC06-76RLO1830 (PNNL), and W-7405-ENG-36 (LANL)) and was supported by the Department of Energy Office of Health and Environ-

mental Research Program under Grants 249311 KP11-01-01 (PNNL) and KP-04-01-00-0 (LANL). This work was supported by the NIH (RR02231) National Stable Isotope Resource at Los Alamos. J.P.Y. and K.M. were supported by Associated Western Universities, Inc., Northwest Division under Grant DE-FG06-92RL-12451 with the U.S. Department of Energy. The research was performed in the Environmental Molecular Sciences Laboratory (a national scientific user facility sponsored by the DOE Biological and Environmental Research) located at Pacific Northwest National Laboratory and operated for DOE by Battelle.

## REFERENCES

1. M. Karplus, Vicinial proton coupling in nuclear magnetic resonance, *J. Am. Chem. Soc.* **85,** 2870 (1963).
2. J. Cavanagh, W. J. Fairbrother, A. G. Palmer III, and N. J. Skelton, "Protein NMR Spectroscopy," Academic Press, San Diego (1995).
3. L. Zhu, B. R. Reid, and G. P. Drobny, Errors in measuring and interpreting values of coupling constants *J* from PE.COSY experiments, *J. Magn. Reson. A* **115,** 206–212 (1995).
4. T. Norwood, and K. Jones, Relaxation effects and the measurement of scalar coupling constants using the E.COSY experiment, *J. Magn. Reson. A* **104,** 106–110 (1993).
5. T. Norwood, The effects of relaxation on the E.COSY experiment, *J. Magn. Reson. A* **114,** 92–97 (1995).
6. C. Griesinger, O. W. Sørensen, and R. R. Ernst, Two-dimensional correlation of connected NMR transitions, *J. Am. Chem. Soc.* **107,** 6394–6396 (1985).
7. L. Mueller, P.E. COSY, a simple alternative to E.COSY, *J. Magn. Reson.* **72,** 191–196 (1987).
8. J. Yang, L. Silks, R. Wu, N. Isern, C. Unkefer, and M. A. Kennedy, Improvements for measuring $^{1}H$–$^{1}H$ coupling constants in DNA via new Stripe-Cosy and Superstripe-Cosy pulse sequences combined with a novel strategy of selective deuteration, *J. Magn. Reson.* **129,** 212–218 (1997).
9. L. Zhu, B. R. Reid, M. A. Kennedy, and G. P. Drobny, Modulation of *J* couplings by cross relaxation in DNA sugars, *J. Magn. Reson. A* **111,** 195–202 (1994).
10. A. Foldesi, S.-i. Yamakage, T. V. Maltseva, F. P. Nilson, P. Agback, and J. Chattopadhyaya, Partially-deuterated nucleotide residues in large DNA duplex simplify the spectral overlap and provide both the J-coupling and nOe informations by the "NMR-window" approach, *Tetrahedron* **51,** 10,065–10,092 (1995).
11. M. A. Delsuc and G. C. Levy, The application of maximum entropy processing to the deconvolution of coupling patterns in NMR, *J. Magn. Reson.* **76,** 306–315 (1988).
12. J. A. Jones, D. S. Grainger, P. J. Hore, and G. J. Daniell, Analysis of COSY cross peaks by deconvolution of the active splittings, *J. Magn. Reson. A* **101,** 162–169 (1993).
13. A. A. Bothner-By and J. Dadok, Useful manipulations of the free induction decay, *J. Magn. Reson.* **72,** 540–543 (1987).
14. P. Huber and G. Bodenhausen, Simplification of multiplets by deconvolution in one- and two-dimensional NMR spectra, *J. Magn. Reson. A* **102,** 81–89 (1993).
15. L. McIntyre and R. Freeman, Accurate measurement of coupling constants by *J* doubling, *J. Magn. Reson.* **96,** 425–431 (1992).
16. V. Blechta, F. Del Rio-Portilla, and R. Freeman, Long-range carbon–proton couplings in strychnine, *Magn. Reson. Chem.* **32,** 134–137 (1994).
17. A. Bax and L. Lerner, Measurement of the $^{1}H$–$^{1}H$ coupling constants in DNA fragments by 2D NMR, *J. Magn. Reson.* **79,** 429–438 (1988).
18. R. K. Harris, "Nuclear Magnetic Resonance Spectroscopy," Longman Scientific Technical, New York (1986).